OPEN

Cell Death and Differentiation (2014) 21, 1575–1587

www.nature.com/cdd

Crucial role of calbindin-D_{28k} in the pathogenesis of Alzheimer's disease mouse model

S-Y Kook[1,6], H Jeong[2,6], MJ Kang[3], R Park[1], HJ Shin[1], S-H Han[1], SM Son[1], H Song[1], SH Baik[1], M Moon[4], EC Yi[3], D Hwang*[,2,5] and I Mook-Jung*[,1]

Calbindin-D_{28k} (CB), one of the major calcium-binding and buffering proteins, has a critical role in preventing a neuronal death as well as maintaining calcium homeostasis. Although marked reductions of CB expression have been observed in the brains of mice and humans with Alzheimer disease (AD), it is unknown whether these changes contribute to AD-related dysfunction. To determine the pathogenic importance of CB depletions in AD models, we crossed 5 familial AD mutations (5XFAD; Tg) mice with CB knock-out (CBKO) mice and generated a novel line CBKO · 5XFAD (CBKOTg) mice. We first identified the change of signaling pathways and differentially expressed proteins globally by removing CB in Tg mice using mass spectrometry and antibody microarray. Immunohistochemistry showed that CBKOTg mice had significant neuronal loss in the subiculum area without changing the magnitude (number) of amyloid β-peptide (Aβ) plaques deposition and elicited significant apoptotic features and mitochondrial dysfunction compared with Tg mice. Moreover, CBKOTg mice reduced levels of phosphorylated mitogen-activated protein kinase (extracellular signal-regulated kinase) 1/2 and cAMP response element-binding protein at Ser-133 and synaptic molecules such as *N*-methyl-D-aspartate receptor 1 (NMDA receptor 1), NMDA receptor 2A, PSD-95 and synaptophysin in the subiculum compared with Tg mice. Importantly, this is the first experimental evidence that removal of CB from amyloid precursor protein/presenilin transgenic mice aggravates AD pathogenesis, suggesting that CB has a critical role in AD pathogenesis.

Cell Death and Differentiation (2014) **21,** 1575–1587; doi:10.1038/cdd.2014.67; published online 23 May 2014

Alzheimer's disease (AD) is a neurodegenerative disorder characterized by the progressive decline of cognition and memory. The major hallmarks of AD include senile plaques and neurofibrillary tangles.[1] The amyloid hypothesis suggests that amyloid β-peptide (Aβ) accumulation is neurotoxic to the cells in the brain regions that have critical roles in learning and memory, including the hippocampus, subiculum, entorhinal cortex and basal forebrain.[2] In addition to the accumulation of Aβ and tau, several neurodegenerative processes of AD in the early stage are accompanied by calcium dysregulation, neuronal death, and mitochondrial and synaptic dysfunction.[2,3] Specifically, disrupted calcium homeostasis has been reported in the brains of AD patients and normal aged subjects.[4,5] Altered levels of calcium (Ca^{2+})-binding proteins could result in impaired Ca^{2+} homeostasis in pathological conditions and disrupted Ca^{2+} signaling, thereby leading to loss of synapses and then dysfunctions of the neural network.[6] We hypothesized that altered expression of a specific Ca^{2+}-binding protein may affect a variety of AD-like pathologies in 5 familial AD mutations (5XFAD) mouse (Tg) brains, in an animal model of AD.

Ca^{2+}-binding proteins maintain calcium homeostasis by buffering excessive intracellular levels of free calcium. Calbindin-D_{28k} (CB) is one of the major calcium-binding proteins that buffer the Ca^{2+} level and transport Ca^{2+}.[7] CB is abundant throughout the central nervous system (CNS) and has been used extensively as a marker of neuronal sub-populations for anatomical and developmental studies. Moreover, CB has been shown to block multiple pro-apoptotic pathways. For example, overexpression of CB inhibited apoptotic activities induced by Aβ and mutant presenilin-1 (PS1) in glial and neuronal cells[8,9] and bax or caspase-3-related apoptotic signaling was increased in uteri of CB knock-out (CBKO) mice.[10] It has been reported that the deficits of learning in mice expressing the familial AD-mutant hAPP correlated strongly with decreased levels of CB in the dentate gyrus of the brain.[11]

[1]Department of Biochemistry and Biomedical Sciences, Seoul National University, College of Medicine, Seoul, Korea; [2]School of Interdisciplinary Bioscience and Bioengineering, Department of Chemical Engineering, POSTECH, Pohang, Korea; [3]Department of Molecular Medicine and Biopharmaceutical Sciences, Graduate School of Convergence Science and Technology and College of Medicine or College of Pharmacy, Seoul National University, Seoul, Korea; [4]Molecular Neurobiology Laboratory, Department of Psychiatry and Mclean Hospital, Harvard Medical School, Belmont, MA, USA and [5]Department of New Biology and Center for Plant Aging Research, Institute for Basic Science, DGIST, Daegu, Korea

*Corresponding author: D Hwang, Department of New Biology and Center for Plant Aging Research, Institute for Basic Science, DGIST, Daegu, 711-873, Republic of Korea. Tel: +82 53 785 1840; Fax: +82 53 785 1809; E-mail: dhwang@dgist.ac.kr

or I Mook-Jung, Department of Biochemistry and Biomedical Sciences, Seoul National University College of Medicine, 28 Yungun-dong, Jongro-gu, Seoul 110-799, Korea. Tel: +82 2 740 8245; Fax: +82 2 3672 7352; E-mail: inhee@snu.ac.kr

[6]These authors contributed equally to this work.

Abbreviations: AD, Alzheimer's disease; Aβ, amyloid β-peptide; CB, calbindin-D_{28k}; 5XFAD, 5 familial Alzheimer's disease mutations; DEP, differentially expressed protein; APP, amyloid precursor protein; PS, presenilin; LC-MS, liquid-chromatography-mass spectrometry; Drp1, dynamin-1-like protein; Fis1, mitochondrial fission 1 protein; Mfn1, mitofusin-1; OPA1, optic atrophy 1; NMDA, *N*-methyl-D-aspartate receptor; ERK, extracellular signal-regulated kinase; MAPK, mitogen-activated protein kinase; CREB, cAMP response element-binding protein

Received 09.9.13; revised 03.3.14; accepted 04.4.14; Edited by N Bazan; published online 23.5.14

Furthermore, homozygous CBKO mice displayed impairments in motor coordination and activity.[12,13] However, whether reduced CB levels in animal models of AD could influence AD pathologies has not been extensively investigated.

To obtain better insights into the pathological significance of these alterations *in vivo*, we generated CB-deficient AD transgenic mice (CBKOTg) and profiled the changes in abundance of proteins and levels of phosphorylation of hundreds of signaling proteins using antibody microarray and mass spectrometry (MS) analysis. From these protein and phosphorylation profiles, we found that the depletion of CB in Tg mice brain elicited significant alterations in cell death pathways, synaptic transmission, mitogen-activated protein kinase (MAPK) signaling and cytoskeleton organization. These results revealed that the removal of CB in Tg mice caused apoptotic features, alteration of mitochondrial dynamic proteins, impaired *N*-methyl-D-aspartate receptor (NMDA)-dependent signaling and decreased synaptic proteins levels at 6 months of age. To summarize, we have first shown, *in vivo*, that the removal of CB in Tg mice may be responsible for aggravating the apoptosis, mitochondrial dysfunction, synaptic alteration on the pathogenesis of AD.

Results

Confirmation of cross-breeding between CBKO and 5XFAD mice for the overexpression of human amyloid precursor protein (APP) and human PS1 genes and the depletion of CB gene. In order to examine the effect of CBKO on AD pathology, we first crossed homozygous CBKO mice with hemizygous Tg and validated production of Tg and homozygous CBKOTg by crossing F1 generation of heterozygous CBKOTg mice. To verify each individual, genomic DNA was then isolated and PCR was performed using primers that span targeted regions of *APP*, *PS1* and *CB* genes (Figure 1a). Based on these results, Tg and CBKOTg mice were identified. In young mice, plaques first appeared and amyloid deposits spread to fill much of the subiculum.[14] CB is widely distributed in the mammalian CNS, including human brains.[7] To confirm the effects of CBKO in the subiculum, we isolated the subiculum (white dotted line) of Tg and CBKOTg mice by an optical microscope (Figure 1b). To determine the protein level of APP, PS1 and CB expression, the offspring of Tg and CBKOTg mice were analyzed and the subiculum homogenates were prepared for immunoblot analysis with anti-APP (6E10), anti-PS1NT and anti-CB antibodies (Figure 1c). We also confirmed the presence of CB and plaque formation in the subiculum of Tg mice, but the absence of CB and the presence of plaque formation in the subiculum of CBKOTg mice by immunohistochemistry (Figure 1d). Taken together, these data showed that all transgenic mice have a number of plaques and mice lacking CB showed a complete depletion of CB in the subiculum with no apparent difference in phenotype.

There was no difference in full-length APP or Aβ accumulation in the subiculum area of CBKOTg compared with Tg mice. Several studies have shown that the density of CB-expressing cells correlates inversely with plaque burden in AD brains.[15,16] To assess whether CB depletion in Tg brains affects Aβ generation, we performed western analysis, ELISA and immunohistochemistry in the subiculum of each individual. Western blot using anti-Aβ antibody (6E10) showed that $\sim$4 kDa bands (monomer form of Aβ) were not significantly altered in CBKOTg mice by CB deletion compared with Tg mice (Figures 2a and b). Moreover, ELISA of insoluble subiculum fractions showed no difference in the amounts of $A\beta_{42}$ between Tg and CBKOTg mice (Figure 2c). Immunohistochemistry for senile plaque in the subiculum, in which the plaque burden was visualized in brain sections using anti-Aβ-specific antibody (4G8), showed that the subiculum lacking CB expression failed to increase total Aβ plaque burden in Tg mice (Figures 2d and e). Consistent with these results, plaque burden did not change in cortical area in both Tg and CBKOTg mice (Supplementary Figure S1). These findings are consistent with the results of ELISA using insoluble fractions between Tg and CBKOTg, indicating that the effect of CB depletion on amyloid pathology was independent of both generation and deposition of Aβ.

Identification of proteins affected by the depletion of CB and their associated cellular biological processes. To examine proteins affected by CB deficiency, we used antibody microarrays to measure abundances of 244 proteins and then to compare their abundances between 6-month-old Tg and CBKOTg subiculum. Among 244 proteins, 31 were identified as differentially expressed proteins (DEPs) between the Tg and CBKOTg subiculum (Supplementary Materials and methods; Supplementary Table S1). Of the 31 DEPs, 13 increased in their abundances in the CBKOTg subiculum, whereas 18 decreased. In particular, p35, PKB/AKT and caspase-3, which are involved in the induction of apoptosis, increased in CBKOTg mice, compared with Tg mice, while anti-apoptosis-related NF-κB (nuclear factor kappa-light chain-enhancer of activated B cells) decreased (Table 1). Moreover, neurofilament 200 and dystrophin, which are involved in organization of cell projection and cytoskeleton, decreased, indicating alteration of cytoskeleton in CBKOTg. These results were also supported by western analysis (Supplementary Figure S2). To further globally investigate the proteome affected by CB deficiency, liquid-chromatography-MS (LC-MS)/MS analysis was performed for the subiculum tissues of Tg and CBKOTg mice. From the samples of Tg and CBKOTg, 3840 and 3970 proteins (a total 4546 proteins) were identified, respectively (Figure 3a). Among them, 3264 were shared. Among the total 4546 proteins, 269 were selected as DEPs (5.92%, Supplementary Table S2; Supplementary Materials and methods). The enrichment analysis of Gene Ontology biological processes (GOBPs) shows that the DEPs are mainly involved in the regulation of apoptosis, synaptic transmission, negative regulation of MAPK activity and mitochondrial fragmentation (Figure 3b; Supplementary Table S3; Supplementary Materials and methods). In addition, cytoskeleton organization, synaptic plasticity, cell cycle and small GTPase-mediated signal transduction also are perturbed in CBKOTg mice compared with Tg mice.

There were fewer NeuN-positive cells in the subiculum of CBKOTg mice than Tg mice at 6 months of age. Although there has been little demonstration of neuronal loss

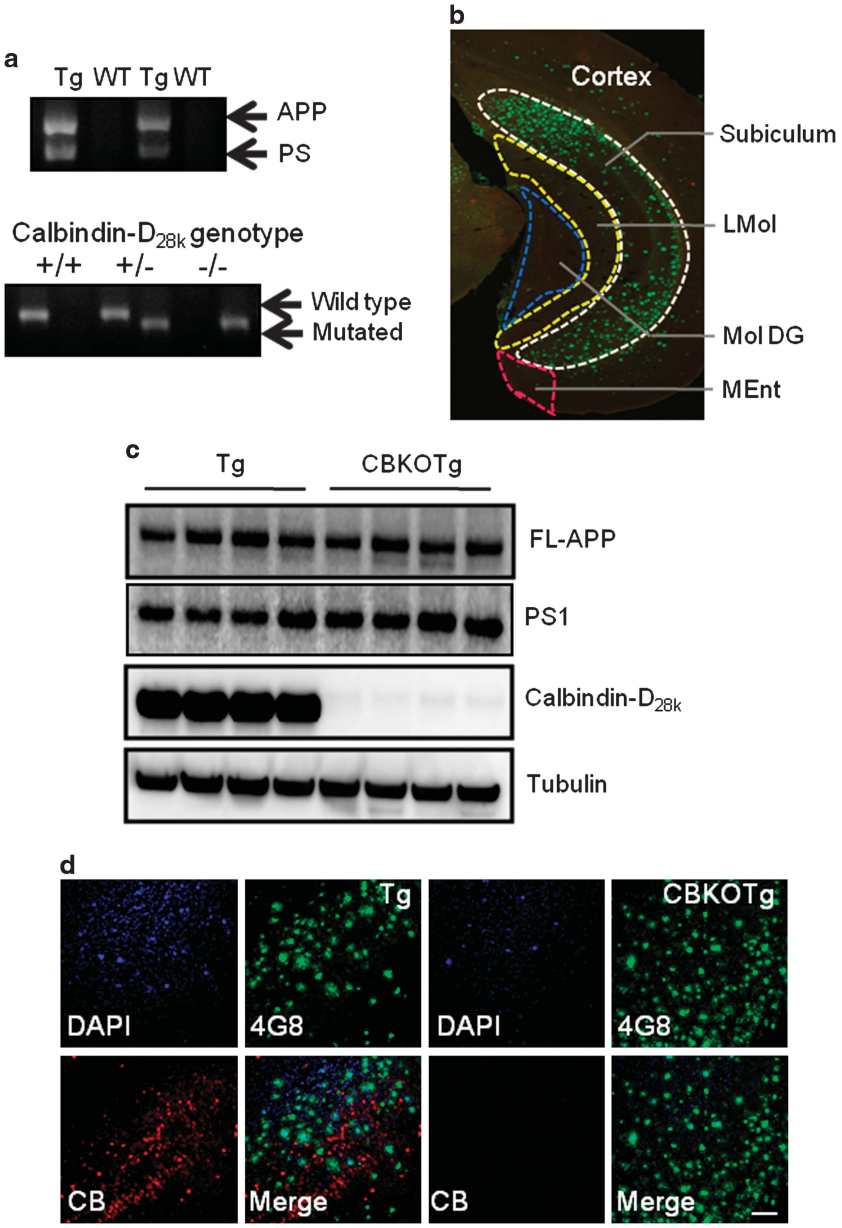

Figure 1 Confirmation of cross-breeding between CBKO and 5XFAD mice for the overexpression of human APP and human PS1 genes and the depletion of CB gene. (**a**) As 5XFAD mice carry the human APP mutation (Swedish, London, Florida) and PS1 (M146L; L286V), transgenic offspring from each line was determined to contain human APP and human PS1. CB expression should have depleted in CBKO mice. These cross-bred mice were analyzed by PCR to determine their gene expression patterns. (**b**) Schematic representation of the subiculum, which is located inside the cortex (the part shown in the white dotted line). LMol, lacunosum moleculare layer; MolDG, molecular layer dentate gyrus; MEnt, medial entorhinal cortex. (**c**) Representative western blot for APP, PS1 and CB expression in the subiculum homogenates from 6-month-old 5XFAD (Tg, $n=4$) and CBKO · 5XFAD (CBKOTg, $n=4$). CB was almost undetectable in subiculum homogenates from CBKOTg mice. (**d**) Coronal serial sections of the brains from 6-month-old mice ($n=4$ for Tg and CBKOTg mice, respectively) were double stained with anti-CB (red) and anti-Aβ (green; 4G8) antibodies, which are imaged by confocal microscopy. Tg mice displayed amyloid plaque deposition (green) and mice lacking CB (CBKOTg) did not show CB expression in the subiculum. Scale bar = 30 μm. Tg: 5XFAD, CBKOTg: CBKO · 5XFAD

in APP transgenic mouse models,[17,18] a recent study showed that 5XFAD mice exhibited extensive neuronal loss by increasing Aβ42 accumulation in cortical layer 5 and the subiculum.[14] Therefore, the role of CB in the neuronal loss was examined in CBKOTg mice using immunohistochemistry of brain sections among nontransgenic littermates, Tg and CBKOTg mice at 6-month-old age with anti-NeuN antibody, a neuronal marker protein. We observed that NeuN-positive cells in the subiculum were visibly reduced in Tg mice compared with littermates (Figure 4a), in agreement with the previous finding.[14] NeuN-positive cells in the subiculum of CBKOTg mice were significantly far fewer and scarcer, compared with both littermate and Tg mice (Figure 4b). To confirm whether the neuronal loss in CBKOTg mice is worse than in Tg mice, we examined NeuN-positive cells at 1.5, 3 and 6-month-old age,

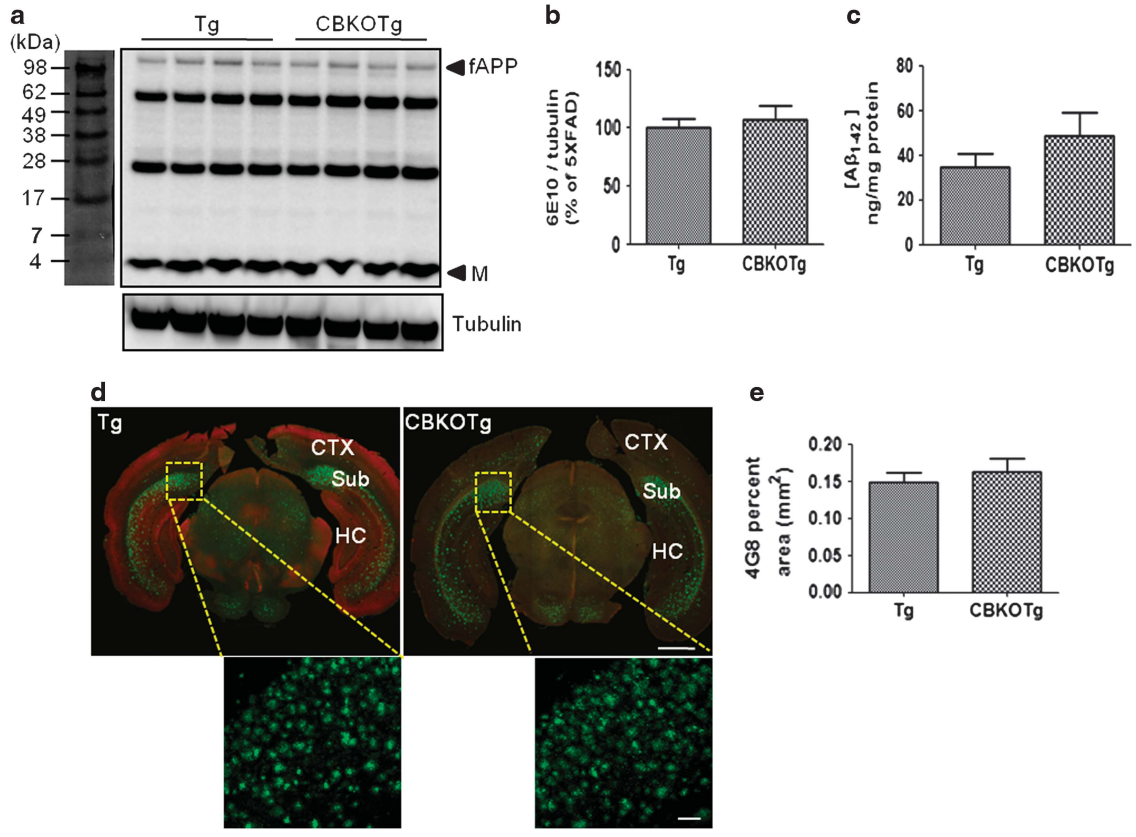

Figure 2 Both full-length APP and Aβ accumulations in CBKOTg mice were unchanged in the subiculum of CBKOTg mice, compared with that of Tg mice. (**a**) Extracts prepared from the subiculum were subjected to immunoblotting and probed with anti-6E10 monoclonal antibody, which detect both full-length APP and Aβ. (**b**) Monomeric Aβ (M) levels were not altered between the groups. Tubulin is a loading control. NS, non-significant. (**c**) 70% FA-insoluble $A\beta_{1-42}$ was extracted from the subiculum and quantified by ELISA for between the groups ($n=4$ for each). CBKOTg mice tend to increase $A\beta_{1-42}$ levels, compared with Tg mice; however, there was no statistically significant difference between CBKOTg mice and Tg mice. (**d**) Representative subiculum regions stained with anti-CB (red) and anti-Aβ (4G8; green) commonly showed Aβ accumulation and the presence or absence of CB. Total Aβ plaque burdens did not differ between the groups. CTX, cortex; HC, hippocampus; Sub, subiculum. Boxed areas are magnified for each figure. Scale bar = 0.6 and 0.1 mm. The section shown is at the level of interaural, 0.36 mm; Bregma, -4.16 mm (Figure 65 in Franklin and Paxinos.[50] (**e**) Percentage of the area occupied by 4G8 was quantified. $n=4$ for Tg and CBKOTg mice, respectively

respectively. Although NeuN-positive cells did not differ between Tg and CBKOTg mice at 1.5-month-old age, NeuN-positive cells of CBKOTg mice from 3 months were seen significantly less than that of CBKOTg mice from 1.5-month-old age (Figures 4c and d). Together, these findings suggest that CB expression could have an important role in preventing the Aβ-induced neurotoxicity and also in maintaining neuronal survival.

Evaluation of apoptosis in the subiculum of CBKOTg mice at 6-month-old age. It was previously shown that mRNA and protein levels of CB were decreased in brains of AD patients and AD mice, respectively.[11,19] CB overexpression has been reported to block apoptotic cell death in lymphocytes, glial cells and the uteri.[9,10,20] However, there is no direct evidence that CB has a role in neuronal apoptosis in AD. To address this question, CBKOTg is one of the best models to show the role of CB in neuronal apoptosis in the brains of Tg mice. The proteomic analyses above revealed that CB deficiency in CBKOTg mice increased significantly the expression of the proteins involved in induction of apoptosis (Figure 3b; Table 1). We investigated whether the expression of apoptosis-related genes is affected by CB depletion in Tg. Interestingly, Bcl-2 and Bcl-xL expression levels were reduced in the subiculum of CBKOTg mice compared with Tg mice (Figures 5a and b). There was no significant change in Bax level. The release of cytochrome *c* (CytC) is tightly controlled by proteins of the Bcl-2 family in the apoptosis pathway.[21] Thus, the release of CytC was then measured by ELISA. We detected a significant increase of CytC in the subiculum of CBKOTg mice (Figure 5c). In addition, significantly higher levels of activated caspase 9 and 3 proteins were detected in the subiculum of CBKOTg mice (Figures 5d and e). To examine quantitatively whether apoptosis occurs in subiculum cells of both Tg and CBKOTg mice, apoptotic cells were assessed by FACS analysis after FITC-annexin V/propidium iodide (PI) staining. Both early (annexin V-positive, PI-negative) and late (annexin/PI-double positive) apoptotic cells were increased in CBKOTg mice than Tg mice, suggesting that CB may have a critical role in cells vulnerable to apoptosis in Tg mice (Figure 5f). These results indicate that apoptotic features increased in response to CB depletion in Tg mice.

Changes of mitochondrial structure and protein levels in the subiculum of CBKOTg mice. Several lines of evidence

Table 1 Antibody microarray analysis of 6-month-old 5XFAD *versus* CBKO · 5XFAD mice

ID	Name	Entrez ID	Symbol	Fold change	*P*-value	Biological function
P9489	p35	12569	Cdk5r1	1.314	0.085[a]	Axon guidance
P1601	PKB/AKT	11651	Akt1	1.826	0.002[a]	Apoptotic mitochondrial changes
S0664	Syntaxin	20907	Stx1a	−1.013	0.984	Synaptic transmission
C8487	Caspase 3 Active	12367	Casp3	1.708	0.019[a]	Apoptotic process
N8523	NF-kB	18033	Nfkb1	−1.719	0.068[a]	Anti-apoptosis
C6974	CAM Kinase IIa	12322	Camk2a	−1.235	0.361	Calcium ion transport
N0142	Neurofilament 200	380684	Nefh	−1.512	0.067[a]	Neurofilament cytoskeleton organization
D8168	Dystrophin	13405	Dmd	−1.475	0.099[a]	Neurotransmitter receptor metabolic process

Antibody microarray analysis of CBKOTg and Tg mice at 6-month of age. The signs of fold changes denote upregulation (positive) and downregulation (negative) by CB depletion. *P*-values represent overall *P*-values computed by the integrative statistical testing method (Materials and methods). Biological functions represent GOBPs assigned to the DEPs by Gene Ontology Consortium. The heat map shows upregulated (red) and downregulated proteins in CBKOTg mice, compared with Tg mice. The color bar denotes the gradient of $\log_2$-fold-changes of the selected DEPs
[a]Significantly upregulated or downregulated molecules (*t*-test *P*-value <0.05, empirical fold test *P*-value <0.05, overall *P*-value <0.1)

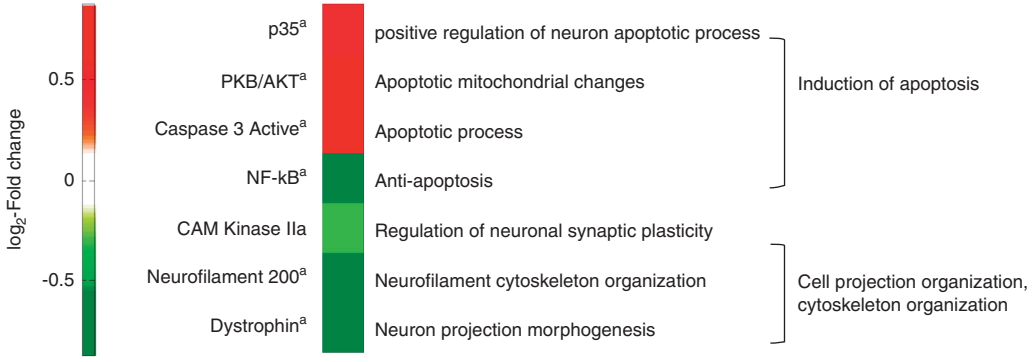

suggest that mitochondrial dysfunction contributes to AD pathogenesis in the brains of transgenic animal models and patients,[22,23] during apoptosis, mitochondria are key organelles that sense and amplify damage[24] and are vital for Ca^{2+} buffering and signal transduction, as well as stress-induced cell death.[25] Also, our proteomic analysis revealed that CB deficiency changed the expression of the proteins involved in mitochondrial fragmentation (Figure 3b). Thus, the structure of mitochondria in the brains of AD mouse models was revealed by EM in previous studies.[26] An EM study to examine the morphological changes of mitochondria in the subiculum of both Tg and CBKOTg mice showed severe cristae disruption like a hole as one of the apoptotic features in CBKOTg mice (Figure 6a). The percentage of elongated and round mitochondria was identified and calculated in each mouse group, and CBKOTg mice showed significantly lower percentage of elongated mitochondria, compared with Tg mice (Figure 6b). Moreover, the length of cristae in CBKOTg mice appeared to be significantly shorter than that in Tg mice (Figure 6c), suggesting that CB may have a role in mitochondrial morphology in CBKOTg mice. Alzheimer's pathology is accompanied by an expression change of the proteins involved in mitochondrial fusion and fission associated with mitochondrial bioenergetics.[27,28] Expression of mitochondrial proteins (dynamin-1-like protein (Drp1), mitochondrial fission 1 protein (Fis1), mitofusin-1 (Mfn1) and optic atrophy 1 (Opa1)) was detected by western blot analysis (Figure 6d). Drp-1 protein expression was significantly higher in CBKOTg mice than Tg mice. The level of Fis1 also tended to increase in the CBKOTg mice although this difference was statistically marginal (Figure 6e). The level of Mfn1 did not differ between Tg and CBKOTg mice. Opa-1 was less in CBKOTg mice than in Tg mice (Figure 6f). These results suggest that CB depletion from Tg mice contributes to the alteration of mitochondrial structure by damaging the mitochondrial cristae and disturbing mitochondrial dynamic remodeling.

Impairment of NMDA receptor-extracellular signal-regulated kinase (ERK) signaling in the subiculum of CBKOTg mice. Our proteomic analysis revealed that CB deficiency changed the expression of the proteins involved in regulation of Ca^{2+} transport and calcium-mediated signaling (Figure 3b). Regulation of intracellular Ca^{2+} concentration is crucial for synaptic plasticity and long-term memory function.[29] $A\beta_{1-42}$ accumulation in brain regions may exacerbate age-related declines in Ca^{2+} regulation that can lead to neuronal dysfunction and subsequent neurodegeneration.[30] The induction of LTP in hippocampal slices requires the activation of NMDA receptors and mice with reduced CB expression show declines in memory and hippocampal LTP.[31,32] To determine whether the effects of changes in NMDA activity on learning and memory may be mediated by CB depletion, we measured the levels of NMDA receptors, synaptic molecules, in the subiculum of both Tg and CBKOTg mice. The levels of NMDA receptor 1 (NR1) and NMDA receptor 2A (NR2A) decreased in the subiculum of CBKOTg mice (Figures 7a and b). We also examined whether reductions of NR1 and NR2A, secondary to CB depletion from Tg mice, would affect NMDA

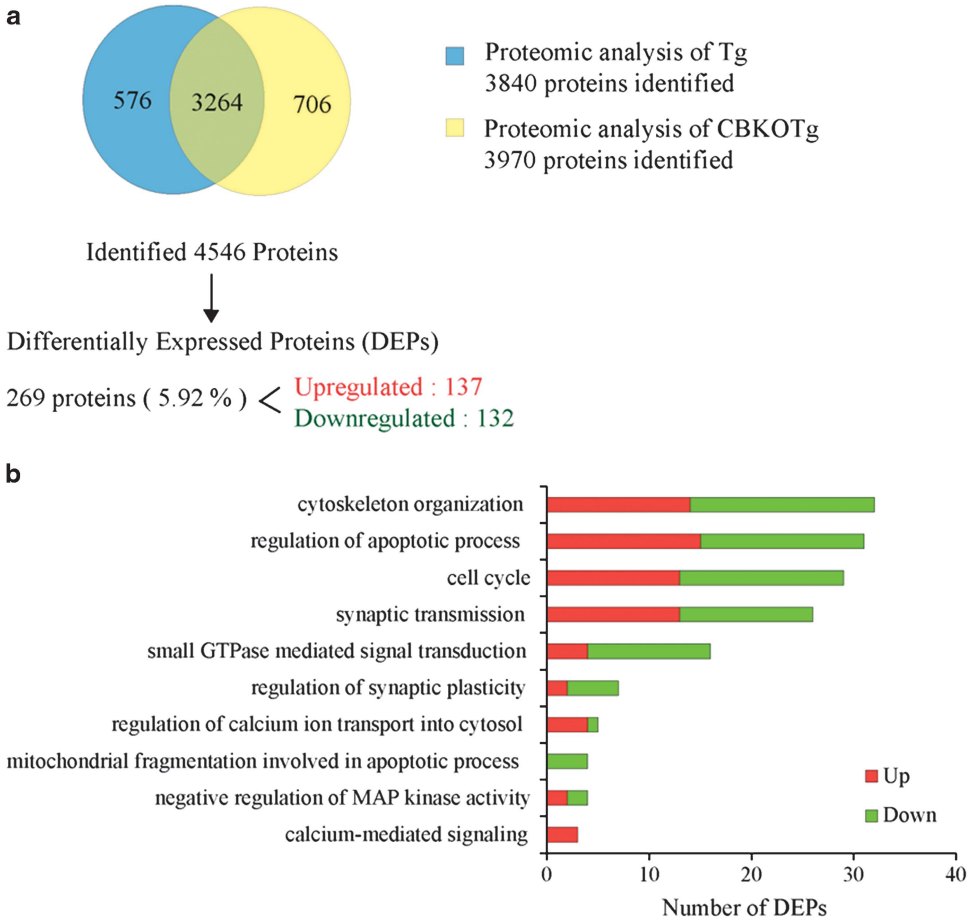

Figure 3 Identification of proteins affected by the depletion of CB and their associated cellular processes. (**a**) Detected proteomes from the subiculum of Tg and CBKOTg mice and DEPs between Tg and CBKOTg mice. In all, 3840 and 3970 proteins (a total 4546 proteins) were identified, respectively (Figure 3a). Among them, 3264 were shared. Among the total 4546 proteins, 269 were selected as DEPs (Supplementary Table S2). (**b**) GOBPs represented by the DEPs. The GOBPs with *P*-value <0.01 from Gene Ontology enrichment analysis were selected as the ones represented by the DEPs (Supplementary Table S3). Among them, the GOBPs associated with AD pathogenesis were selected and shown here (see Supplementary Table S4 for the proteins involved in these GOBPs). The numbers of DEPs involved in the selected GOBPs were displayed (red: upregulated DEPs; green: downregulated DEPs; Supplementary Table S4)

receptor-mediated signaling pathways. In particular, the activation/phosphorylation of ERK is regarded as a key biochemical event in cognition. Our proteomic analysis also showed that CB deficiency changed the expression of the proteins involved in regulation of MAPK pathway (Figure 3b). The ERK activation leads to activation of cAMP response element-binding protein (CREB), a transcription factor linked to the formation of long-term memory.[33] Especially, NMDA receptors enhance learning and memory through the activation of CREB by phosphorylation at serine 133.[34] The levels of phosphorylated ERK1/2 and CREB at serine 133 significantly decreased in CBKOTg mice, compared with Tg mice (Figures 7a and c), whereas the levels of total ERK1/2 and CREB showed no change. We found that the immunoreactivity of phosphorylated CREB decreased in neurons of CBKOTg subiculum, compared with those in Tg mice (Figure 7d). Merged images of anti-NeuN and anti-pCREB stainings showed decreased yellow fluorescence in CBKOTg mice, and these images were quantified based on the fluorescence intensity (Figure 7e), suggesting that CREB inactivation is enhanced by CB depletion. To investigate whether CB depletion has any additive effects on the levels of synaptic proteins, we measured the levels of PSD-95 and synaptophysin in the subiculum of both CBKOTg and Tg mice. PSD-95 levels were reduced by 15% in CBKOTg mice and synaptophysin levels also decreased in the subiculum of CBKOTg by 24%, compared with Tg mice (Figures 7f and g). These data provide evidence that CB depletion has an important role in regulating of synaptic transmission and plasticity in Tg mice.

Discussion

The pathological features of AD have been reported to include Aβ deposition, disrupted Ca^{2+} homeostasis, cell death and reduction of synaptic proteins. In this study, we have demonstrated that CB depletion contributes to Aβ-induced apoptosis and neurodegenerative changes in the brains of AD animal model. These results are consistent with earlier report that CB protein levels were markedly reduced in human AD brains and rodent AD model brains.[11] To test the hypothesis

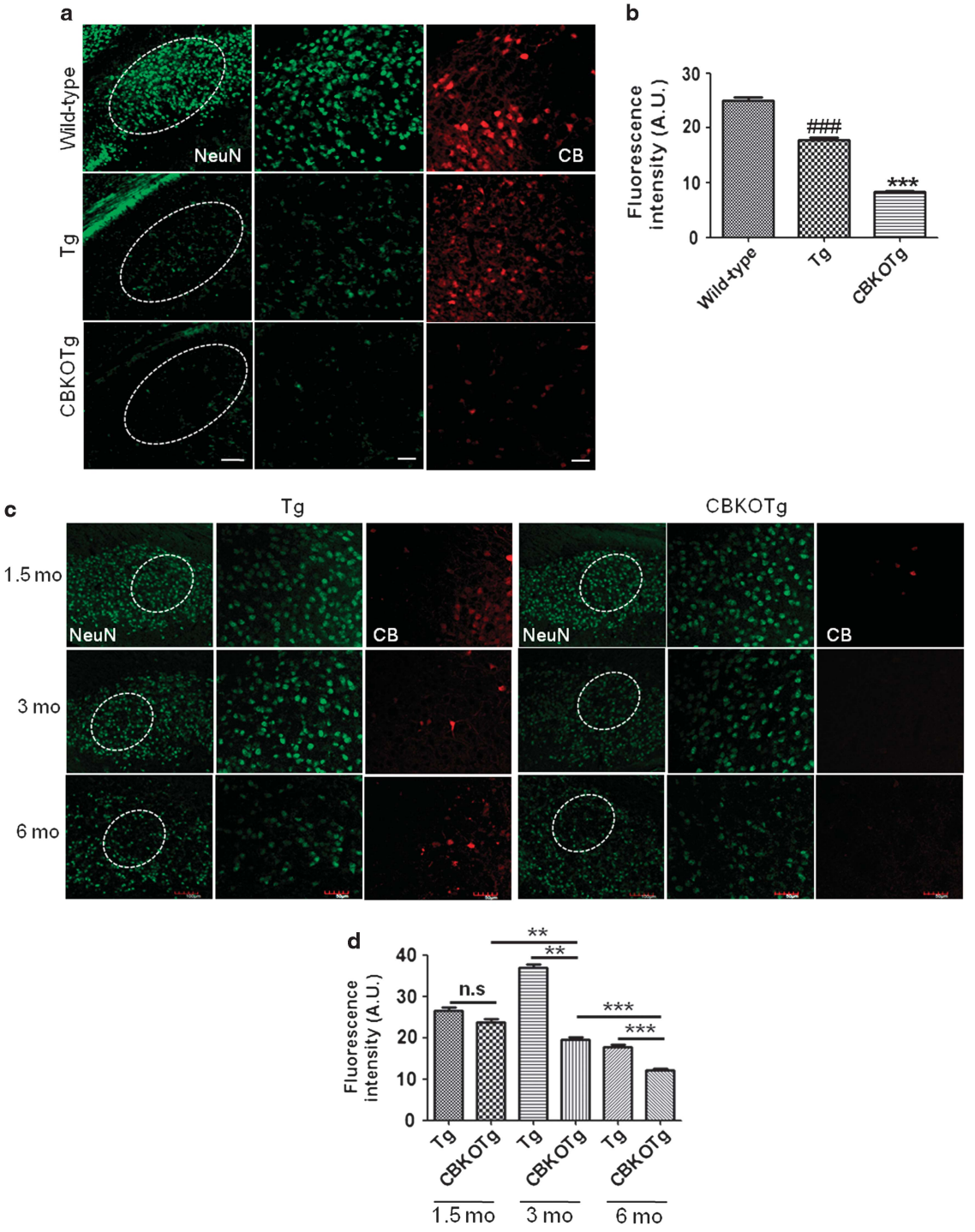

Figure 4 There were fewer NeuN-positive cells in the subiculum of CBKOTg mice compared with Tg mice at 6 months of age. Coronal serial brain sections from 6-month-old mice ($n=4$ for littermates, Tg and CBKOTg mice, respectively) were costained with anti-NeuN (green) and anti-CB (red) antibodies, which were imaged by confocal microscopy. Shown are micrographs of in the subiculum (areas within dashed line in left panels) and respective higher magnification images (middle panels) (**a**) CB levels are significantly reduced in CBKOTg mice compared with littermates and Tg mice (right panels). Neurons are significantly reduced in the number in the subiculum of Tg mice, compared with littermates. The quantity of neurons in the subiculum of CBKOTg mice were significantly less, compared with the subiculum of Tg mice. Scale bar = 100 μm in left panels, scale bar = 50 μm in middle panels. (**b**) Fluorescence intensity of NeuN-positive cells were decreased by 30% in Tg mice compared with WT mice, and an intensity was further decreased in CBKOTg mice to $\sim$50%. (**c**) Coronal serial brain sections from 1.5, 3 and 6-month-old mice ($n=4$ for Tg and CBKOTg mice) were costained with anti-NeuN (green) and anti-CB (red) antibodies, which were imaged by confocal microscopy. Although NeuN-positive cells of Tg were similar to them of CBKOTg at 1.5-month-old mice, NeuN-positive cells were less in CBKOTg than Tg at 3-month-old mice. (**d**) Fluorescence intensity of NeuN-positive cells in CBKOTg mice was reduced significantly compared with Tg mice from 3-month-old mice. Scale bar = 100 μm in left panels, scale bar = 50 μm in middle panels. $^{###}P<0.001$, Tg *versus* Littermate; $^{**}P<0.01$ and $^{***}P<0.001$, CBKOTg *versus* Tg mice

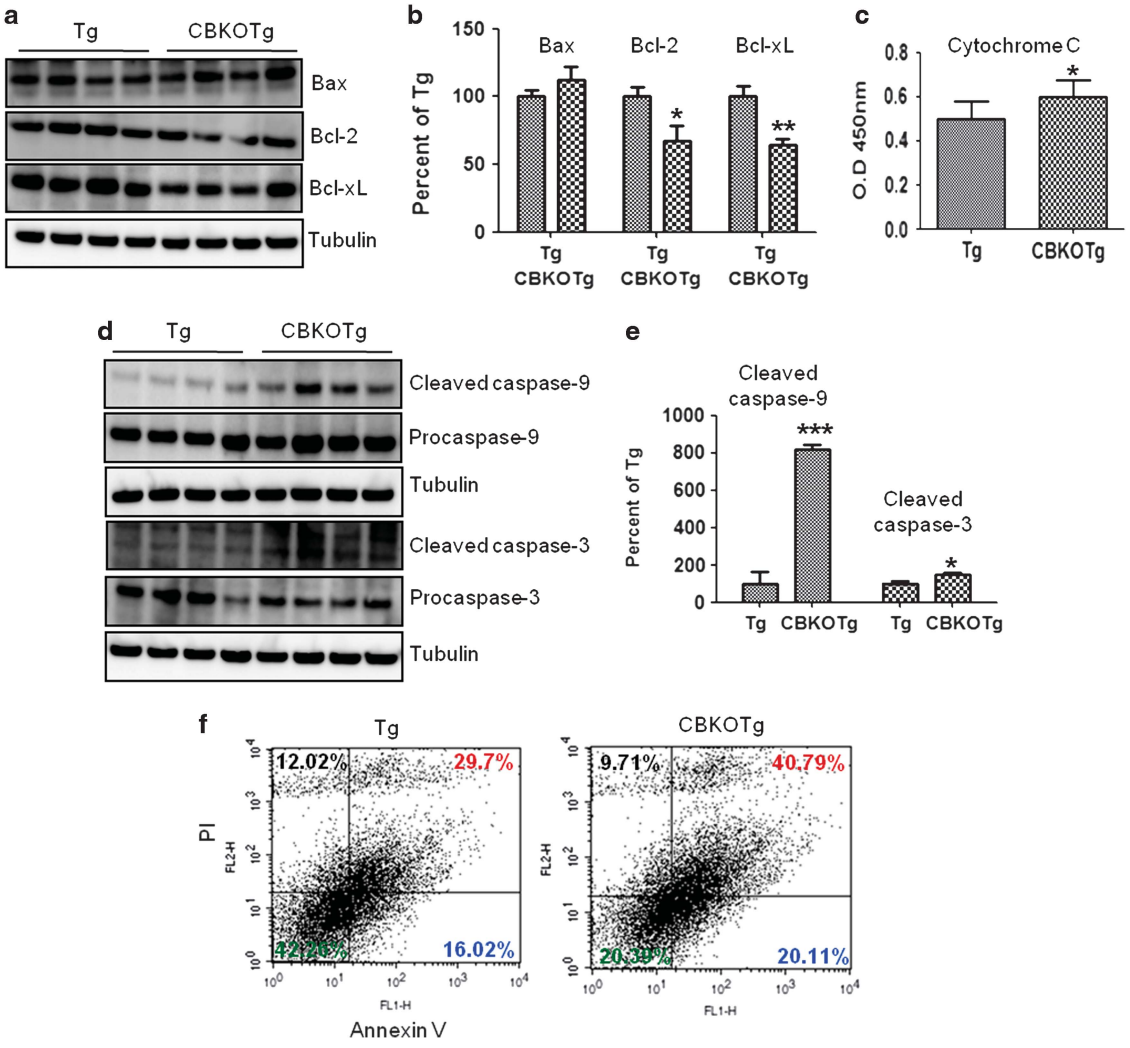

Figure 5 Evaluation of apoptosis in the subiculum of CBKOTg mice at 6 months of age. (**a**) Bax, Bcl-2 and Bcl-xL expression levels were analyzed by western analysis in the subiculum from 6-month-old Tg ($n=4$) and CBKOTg mice ($n=4$). Tubulin was a loading control. (**b**) Bcl-2 and Bcl-xL levels were significantly decreased in CBKOTg mice compared with Tg mice. No changes were detected for Bax levels. Protein levels were normalized against tubulin. (**c**) CytC ELISA assay was performed in cytosolic extracts of the subiculum, and CytC levels in CBKOTg mice increased significantly, compared with Tg mice. (**d**) Expression levels of cleaved caspase-9 and caspase-3 was measured by western analysis. $n=4$ for Tg and CBKOTg mice, respectively. (**e**) Activated caspase forms increased significantly in CBKOTg mice than Tg mice. Cleaved forms of proteins were normalized to its precursor form and are shown as a percent of Tg mice. (**f**) Subiculum extracts were homogenized with binding buffer and were subjected to FACS analysis after propidium iodide (PI: Y axis) and annexin V (X axis) staining. Note that CB deletion increased from early apoptotic cells (lower right quadrant) to late apoptotic cells (upper right quadrant) in Tg mice. Three independent experiments were performed with 10 000 cells. *$P<0.05$, **$P<0.01$ and ***$P<0.001$. CBKOTg *versus* Tg mice

that the removal of CB from 5XFAD mice may contribute to the pathogenesis of AD, we generated CBKO AD transgenic mice (CBKOTg) as an *in vivo* experimental model with depleted CB expression (Figure 1). Pasti *et al.*[35] demonstrated that inhibition of CB expression lead to prolonged increase of intraneuronal Ca^{2+} after NMDA or potassium stimulation of hippocampal slices.[35] Greene *et al.*[36] showed that CB-expressing cells in the brain of AD patients were unaffected by and resistant to degeneration.[36] As a consequence of CB deficiency in the brains of Tg mice, we first demonstrated significant alterations in cell death pathways, synaptic transmission and MAPK signaling pathways from our initial antibody array analysis (Table 1). By MS, functional enrichment analysis also showed that the DEPs between both Tg and CBKOTg mice were significantly involved in apoptosis induction, synaptic transmission, MAPK activity and mitochondrial dysfunction (Figure 3). Based on these analyses, we have provided compelling evidence that CB depletion could alter pathological features of AD, independent of Aβ generation, evidenced from both biochemical experiments and immunohistochemistry. Although there was no difference in Aβ accumulation between Tg and CBKOTg mice, severe neuronal loss was found in the subiculum of CBKOTg mice, compared with that of Tg mice. Greater atrophy in the subiculum is associated with increased risk of conversion from mild cognitive impairment to AD.[37] We also found that anti-apoptotic proteins, such as bcl-2 and bcl-xL, significantly decreased and the release of CytC with activation of caspase-9 and caspase-3 increased in the brains of CBKOTg mice. In addition, FACS analysis showed that both early

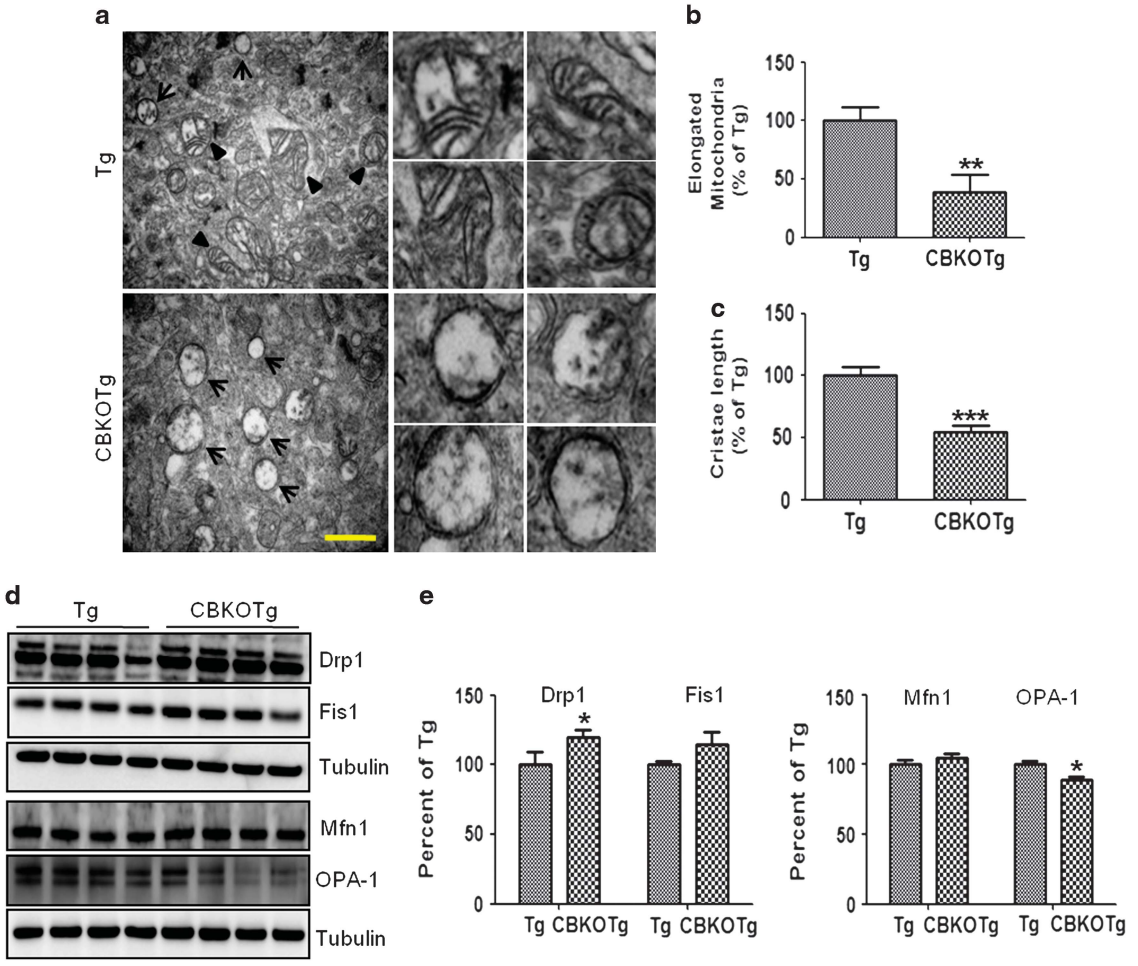

Figure 6 Changes of mitochondrial structure and protein levels in the subiculum of CBKOTg mice. (**a**) Representative EM images showed mitochondria in the subiculum of Tg and CBKOTg mice at 6 months of age. Arrowheads indicate mitochondria with cristae. Abnormal mitochondria without cristae are marked by arrows. Although altered mitochondria were observed in Tg mice, there were more altered mitochondria in CBKOTg mice than Tg mice ($n=4$ for Tg and CBKOTg mice, respectively). Scale bar $=1\ \mu$m. (**b**) Elongated mitochondria were counted and calculated as the percent of elongated mitochondria ($n=9$ mitochondria images per each group). (**c**) Analysis of the length of mitochondria cristae was performed ($n=25$ mitochondria per each group). (**d**) Subiculum extracts were probed for Drp1, Fis1, Mfn1, OPA-1 and tubulin. The level of Drp1 increased in CBKOTg mice, compared with Tg mice, and OPA-1 was reduced. The level of Fis1 slightly increased in CBKOTg mice than Tg mice, but was not statistically significant. No changes were detected in Mfn1 levels ($n=4$ independent extracts per group). (**e** and **f**) Quantification of Drp1, Fis1, Mfn1 and OPA-1 protein levels in (**d**). Tubulin is a loading control. $^{*}P<0.05$, $^{**}P<0.01$ and $^{***}P<0.001$. CBKOTg *versus* Tg mice

(annexin V-positive, PI-negative) and late (annexin/PI-double positive) apoptotic cells increased in CBKOTg mice, compared with Tg mice (Figure 5). These findings are consistent to earlier reports that CB protects against apoptotic cell death brought on by Aβ in both neuronal and glial cells, and that bax and caspase-3 proteins are upregulated by CBKO in the murine uterus.[8–10] Therefore, it is reasonable to suggest that CB expression may contribute to neuronal survival in Tg mice. During apoptosis, remodeling of the mitochondrial cristae is accompanied by fragmentation of the mitochondria network.[21,38] The EM images showed that mitochondria of CBKOTg mice represent fragmentation and cristae disruption compared with Tg mice. Currently, it is believed that the overall shape of mitochondria is controlled by the balance between fusion and fission events that are mediated by specific proteins.[39] Defects in mitochondrial fusion and fission proteins are associated with a wide range of neurodegenerative diseases.[40] Interestingly, protein levels of both Drp1 and OPA1, one of the fission and fusion proteins, were significantly altered in CBKOTg mice compared with Tg mice (Figures 3 and 6), suggesting that the altered mitochondrial dynamics affects mitochondrial morphology as well as their functions, which lead to neuronal apoptosis in CBKOTg mice. The integrity of mitochondrial cristae during apoptosis is maintained not only by Opa1, but also by the genetic inhibition of Drp1.[41] Thus, the altered Drp1 and Opa1 protein levels of CBKOTg mice support cristae disruption. Although the inhibition of CB expression impaired water maze learning in antisense for CB transgenic mice,[32] whether CB depletion affects the mechanism associated with memory function has not been determined. The NMDA receptors consisting of two NR1 and two NR2 subunits are well-known key molecules for regulating memory function and synaptic plasticity.[42] Protein levels of NR1 and NR2A are reduced in the brains of CBKOTg mice, compared with Tg mice. ERK1 and ERK2 are highly expressed in the adult mammalian CNS, and their activation

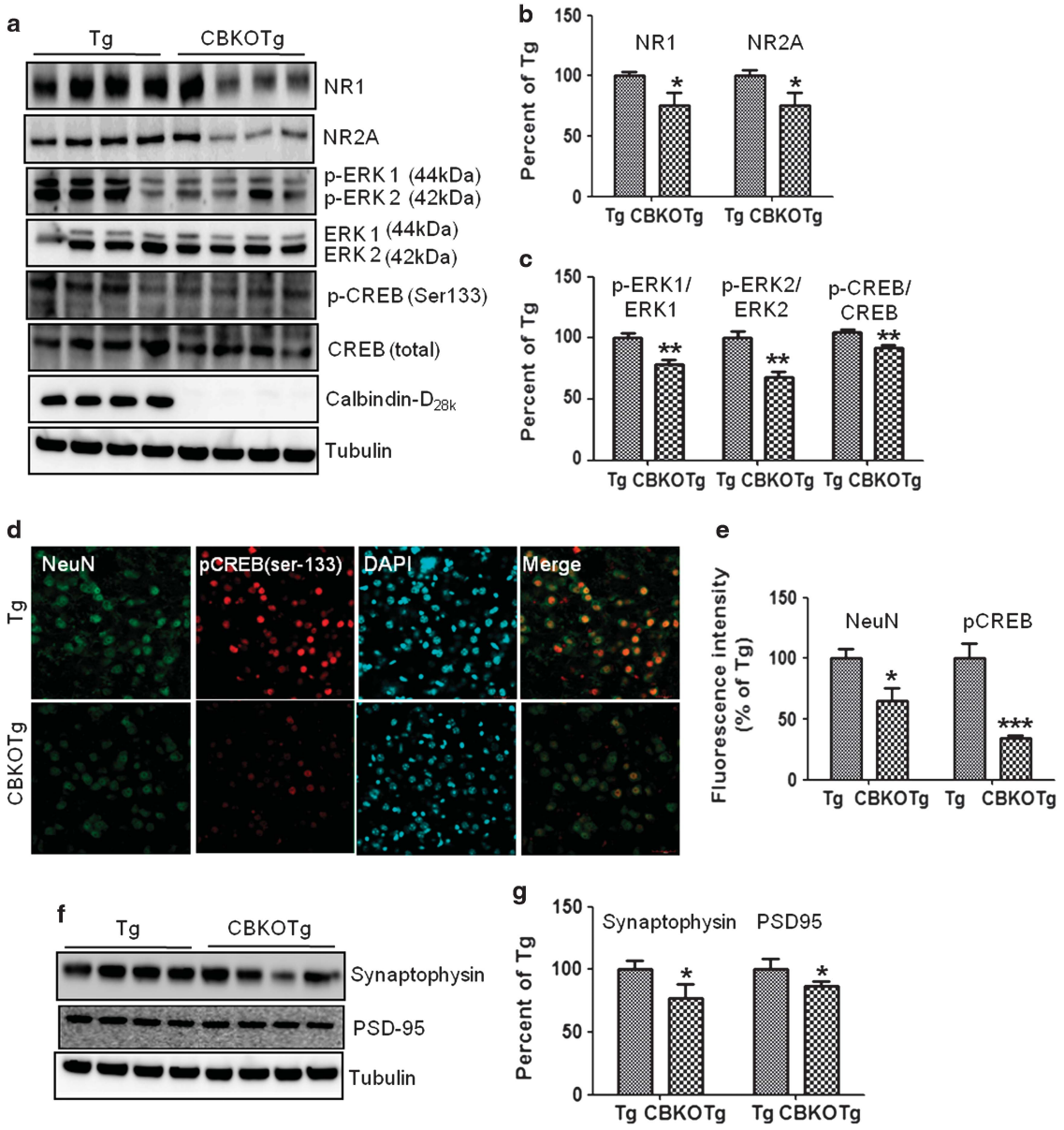

Figure 7 Impairment of NMDA receptor-ERK signaling in the subiculum of CBKOTg mice. (**a**) Subiculum extracts of both Tg and CBKOTg mice were prepared for immunoblotting with anti-NR1, anti-NR2A, anti-pERK1/2, anti-ERK1/2, anti-pCREB (Ser-133), anti-CREB and anti-tubulin antibodies. Equivalent amounts of proteins from individual samples were analyzed by western blotting, and tubulin was used as a loading control. (**b** and **c**) Quantification of NR1, NR2A, pERK/ERK and pCREB/CREB. NR1and NR2A protein levels were significantly reduced in CBKOTg mice than Tg mice. Moreover, phosphorylations of ERK1/2 and CREB decreased significantly in CBKOTg mice than Tg mice. (**d**) Immunostainings of both NeuN (green) and phospho-CREB (red). Phospho-CREB expression decreased in NeuN-positive subiculum cells of the brains of CBKOTg mice than in those of Tg mice. Green: NeuN, red: phospho-CREB, blue: DAPI staining for nucleus. Scale bar = 30 μm. (**e**) Fluorescence intensity of NeuN and phospho-CREB in CBKOTg mice decreased significantly compared with Tg mice. (**f**) Subiculum homogenates from the brains of both Tg and CBKOTg mice prepared for immunoblotting with antibodies against postsynaptic proteins, PSD-95 and presynaptic protein, and synaptophysin. (**g**) Quantification showed decreased levels of synaptophysin and PSD-95 in CBKOTg mice compared with Tg mice ($n = 4$ for Tg and CBKOTg mice, respectively). $^{*}P < 0.05$ and $^{**}P < 0.01$. CBKOTg *versus* Tg mice

relies on Ca^{2+} influx via the NMDA receptor, which is regarded as a key biochemical event in cognition through activation of CREB.[33,43,44] Activation of both ERK1/2 and CREB was decreased by the removal of CB in the brains of Tg mice (Figures 7a and c). We also confirmed that immunohistochemical staining of brain sections for phosphorylated CREB revealed a decrease in subiculum neurons of CBKOTg mice, compared with those in Tg mice (Figures 7d and e). These results raise the possibility that CB depletion contributes to neuronal deficits and cognitive dysfunction in Tg mouse models, and persistent mitochondrial fission could lead to synaptic damage, bioenergetic failure and subsequent neurodegeneration.[45,46] Another interesting finding in this study is the influence of CB on synaptic protein levels. Loss of synaptic function is a key characteristic of AD progression, because it is directly linked with cognitive impairment.[47]

A growing body of evidence that CB is an important regulator of synapses has been reported. First, CB is expressed in distinct cell types throughout the CNS, buffers intracellular Ca^{2+} and modifies synaptic functions in neurons.[7] Second, overexpression of CB has been shown to increase neuronal differentiation and neurite growth.[48] Finally, recent evidence suggests that CB binds directly to caspase-3 and inhibits its activity in osteoblasts, and caspase-3 then triggers early synaptic dysfunction in a Tg2576 AD mouse model.[49,50] We have found decreased protein levels of PSD95 and synaptophysin, the presynaptic and postsynaptic proteins (Figures 7f and g). Therefore, the alterations in both presynaptic and postsynaptic proteins imply that CB depletion may be important in the regulation of synapse formation.

In summary, we have revealed for the first time that CB has a critical role *in vivo* in the apoptotic features, including mitochondria alteration as well as loss of synaptic proteins, in a AD mouse model. Our findings suggest that the CB depletion may be an important contributor to the pathogenesis of AD by exacerbating neuronal loss, apoptotic cell death, mitochondrial dysfunction and synaptic loss.

Materials and Methods

Animals. Female transgenic mice with 5XFAD were purchased from Jackson Lab (Bar harbor, ME, USA). These mice co-express and co-inherit FAD mutant forms of human APP (Swedish mutation: K670N, M671L; Florida mutation: I716V and London mutation: V717I) and PS1 (M146L; L286V) transgenes under transcriptional control of the neuron-specific mouse Thy1 promoter.[14,51] Heterozygous Tg transgenic mice (B6/SJL hybrid background) were cross-bred with CB homozygous knockout (CBKO) mice.[12] The resultant F1 heterozygous $CB^{+/-}$ Tg mice were further intercrossed, yielding animals with four different genotypes (wild-type, Tg, CBKO · WT and CBKOTg) in the F2 progeny. All experiments were done with these mice at 6 months of age. Subiculum tissues were rapidly excised from the brains of the killed mice by using optical microscopy for protein isolation. Some subiculum tissues were fixed in cold 2.5% glutaraldehyde for electron microscopy (EM). Animal treatment and maintenance were carried out in accordance with the Guide for the Care and Use of Laboratory Animals (NIH publication No.85-23, 1985 edition) and the Animal Care and Use Guidelines of Seoul National University, Seoul, Korea. All efforts were made to minimize animal suffering and to reduce the number of mice used.

Genotyping of Tg and CBKO mice. CBKO mice were provided by Professor Sukho Lee (Seoul National University, College of Medicine, Seoul, Korea). Genomic DNA was obtained from the ears by digestion buffer (50 mM Tris-HCl, 20 mM NaCl, pH 8.0, 1 mM EDTA, 1% SDS, 20 mg/ml Proteinase K) at 55 °C for 2 h, followed by phenol and isopropanol. Polymerase chain reaction (PCR) was performed with a separate set of primers designed for each allele to distinguish the CB WT from CB mutant alleles. The oligonucleotide primers designed for the CB WT allele were as follows: upstream, 5′-TCCCTCACCTA-GAGATAGAAGCAGCGCAG-3′; downstream, 5′-AGACAGCAGAATCGAGGAG TCTGCTGCTC-3′. The oligonucleotide primers designed for the CB mutant allele were as follows: upstream, 5′-TCCCTCACCTAGAGATAGAAGCAGCGCAG-3′; downstream, 5′-GCTAAAGCGCATGCTCCAGACTGCCTTGG-3′. The size of the WT PCR product was 254 bp and the mutant PCR product was 192 bp.

Immunohistochemistry. For immunohistochemistry, WT, Tg, CBKO · WT and CBKOTg ($n=4$ each) mice were killed at 6 months of age. Mice were anesthetized with a mixture of Zoletil 50 (Virbac, Carros, France) and Rompun (Bayer Korea, Seoul, Korea) solution (3 : 1 ratio, 1 ml/kg, i.p.) and perfused transcardially with a freshly prepared solution of 4% PFA in PBS. After the mice were decapitated, brains were dissected from the skull. Serial 30-μm thick coronal tissue sections were cut using a freezing microtome (Leica, Nussloch, Germany). Free-floating sections were incubated with the following the primary antibodies; biotin-labeled 4G8 (1 : 700; Covance, Princeton, NJ, USA), rabbit anti-CB (1 : 3000; Swant, Bellinzona, Switzerland), mouse anti-neuron-specific nuclear protein (NeuN) antibody (1 : 2000; Millipore, Schwalbach, Germany) and rabbit anti-phospho-CREB Ser 133 antibody (1 : 800; Cell Signaling Technology, Beverly, MA, USA) overnight at 4 °C. After washes in PBS, the sections were incubated with the following secondary antibodies; Alexa Fluor 488-conjugated streptavidin (1 : 1000; Invitrogen, Carlsbad, CA, USA), goat anti-rabbit Alexa 594 (1 : 1000; Invitrogen and donkey anti-mouse Alexa 488 antibody (1 : 1000; Invitrogen) for 2 h. All sections were counterstained with DAPI (4′-6-diamidino-2-phenylindole) before mounting and analyzed on a confocal laser scanning microscopy (FluoView FV 10i; OLYMPUS, Center Valley, PA, USA).

Antibody microarray and statistical analysis. Subiculum extracts of 6-month-old Tg and CBKOTg mice ($n=3$ each) were subjected to Panorama Antibody Microarray Cell Signaling (Sigma-Aldrich, St. Louis, MO, USA) analysis consisting of 224 different antibodies according to the manufacturer's instructions. Briefly, Cy3 and Cy5 dye (Amersham, Little Chalfont, Buckinghamshire, UK) were attached to proteins extracted from Tg and CBKOTg mice. Next, equal amounts of labeled proteins from Tg and CBKOTg subiculum were mixed together and hybridized to antibody microarrays. After washing, the microarrays were scanned at wavelengths of 532 nm (Cy3) and 635 nm (Cy5) to detect signals using a GenePix4008B Scanner (Molecular Devices, Sunnyvale, CA, USA), and data were analyzed by GenePix software (Molecular Devices). Lowess normalization was performed for four signals of each protein.[52] Normalized signals for four replicates of one protein between CBKOTg and Tg mice were compared to identify DEPs using an integrative statistical testing method[53] in which adjusted *P*-values for each protein were calculated using both Student's *t*-tests and median fold-change test and then combined to compute overall *P*-values using Stouffer's method.[54] Proteins with overall *P*-values <0.1, *P*-values of *t*-test <0.05 and *P*-values of median fold test <0.05 were selected as DEPs by the depletion of CB.

In-gel digestion. Hippocampal subiculum tissue lysates were prepared by sonication followed by solubilization in lysis buffer consisting of 50 mM Tris/HCl pH 8.0, 1% SDS, 50 mM sodium fluoride, 1 mM sodium orthovanadate and complete protease inhibitor cocktail (Roche Diagnostics, Mannheim, Germany). Protein concentrations were measured using a Micro BCA Protein Assay Kit (Thermo Scientific, Rockford, IL, USA). Solubilized proteins were boiled in SDS sample buffer (Invitrogen), fractionated by SDS-PAGE (4–12% Bis-Tris Gel, Invitrogen) and stained with Coomassie Brilliant Blue (Sigma-Aldrich). Protein gel regions were cut and subjected to in-gel tryptic digestion following the general protocol.[55] Briefly, protein gels were excised, destained and washed. Proteins were reduced with 20 mM dithiothreitol and alkylated with 55 mM iodoacetamide. After dehydration with acetonitrile, the proteins were digested with 13 ng/μl sequencing grade modified porcine trypsin (Promega, Madison, WI, USA) in 50 mM ammonium bicarbonate overnight at 37 °C. Peptides were extracted from the gel pieces with 5% (v/v) acetonitrile in 0.1% (v/v) formic acid and 50% (v/v) acetonitrile in 0.1% (v/v) formic acid. The eluates were dried under vacuum and stored at -20 °C until used.

LC-MS/MS analysis. Peptides isolated from the in-gel digestion were resuspended in 50 μl of solvent A (2% acetonitrile in 0.1% formic acid) and 2 μl of sample was injected into nano-HPLC system (Easy nLC; Thermo Fisher Scientific, San Jose, CA, USA) and LTQ-Velos mass spectrometer (Thermo Fisher Scientific). The sample was loaded onto an in-house packed 75 μm (inner diameter) $\times$ 10 cm C_{18} column and separated with a linear gradient of 2–38% solvent B (98% acetonitrile in 0.1% formic acid) for 90 min at a flow rate of 300 nl/min. Standard mass spectrometric condition of the spray voltage was set to 1.9 kV and the temperature of the heated capillary was set to 325 °C. The LTQ was operated in data-dependent mode with one survey MS scan at the mass range 400–1400 m/z and followed by five MS/MS scans. Precursor ions were dynamically excluded for a period of 30 s.

Protein identification and quantification. LC-MS/MS raw data were searched by SEQUEST algorithm against forward–reverse ipi.MOUSE.v3.87 using the following parameters: 1.5 Da precursor mass tolerance; 1.0 Da product ion mass tolerance; semitryptic digestion; up to two missed cleavages; variable modifications: oxidation of methionine ($+15.99$); fixed modifications: carbamidomethylation of cysteine ($+57.02$). The SEQUEST search results were evaluated by computing the probability for each identified peptide using TPP v.4.5b.[56] Peptides with false discovery rate <0.005 were regarded as reliably identified peptides and matched to proteins using the ProteinProphet software.[57] Proteins with the protein probability ≥ 0.9 were regarded as reliably identified proteins and

quantified using a spectral count-based method proposed by Fu *et al.*[58] For each protein, the spectral counts between CBKOTg and Tg mice were compared to compute a spectral index (SPI), a measure of fold-change of the spectral counts, as described in Fu *et al.*[58] To assess the statistical significance of a SPI value for each protein, an empirical distribution of SPI was estimated by performing 1000 random permutation experiments. For a SPI value for each protein, *P*-value was computed by a two- tailed test using the empirical distribution. Proteins with (1) SPI *P*-value <0.05 and (2) the number of identified unique peptides ≥ 2 in one of Tg and CBKOTg mice were identified as DEPs.

Enrichment analysis of GOBPs. To identify cellular processes represented by the DEPs, the enrichment analysis of GOBPs was performed using MetaCoreTM (ver 6.7; Thomson Reuters, New York, NY, USA), which provides *P*-value as the significance of each GOBP being enriched by the DEPs.[59] The GOBPs with *P*-value <0.01 were selected as the ones significantly represented by the DEPs.

Aβ ELISA. Human Aβ_{42} levels were quantified with a commercially available ELISA kit using an anti-Aβ_{42} C-terminal-specific antibody according to the manufacturer's protocol (Immuno Biochemical Laboratories Co., Gunma, Japan). Extracts of brain subicular tissues were lysed by sonication with PBS containing protease inhibitor cocktails (Sigma-Aldrich). The homogenates supplemented with 70% formic acid were sonicated for 35 s and ultra-centrifuged at 100 000 $\times$ *g* for 1 h at 4 °C. The formic acid extracts were neutralized with 1 M Tris phosphate buffer (pH 11) and then diluted with the ELISA sample buffer (1 : 20). ELISA plates were developed using a color reaction, and the absorbance was read at 450 nm using a plate reader (POWER-XS; BIO-TEK, Winooski, VT, USA).

Transmission EM (TEM). Several subiculum pieces from Tg and CBKOTg were randomly excised, diced (1 mm^3), then fixed in a mixture of 2.5% glutaraldehyde in 0.1 M phosphate buffer (pH 7.2) and 2% paraformaldehyde in 0.1 M phosphate or cacodylate buffer (pH 7.2) and embedded with epoxy resin at 4 °C for overnight. The epoxy resin-mixed samples were loaded into capsules and polymerized at 38 °C for 12 h and 60 °C for 48 h. Thin sections were sliced on an ultramicrotome (RMC MT-XL) and collected on a copper grid. Appropriate areas for thin sectioning were cut at 65 nm and stained with saturated 4% uranyl acetate and 4% lead citrate. The ultrastructure of mitochondria of the brain was then examined by a TEM (TEM-1400, Tokyo, Japan). Mitochondria were measured and the averages were determined ($n=10$ for each group).

Western blot analysis. Mouse brains were lysed in RIPA buffer (50 mM Tris-Cl, pH8.0, 150 mM NaCl, 1% NP-40, 0.5% Na-Doc, 0.1% SDS) containing protease inhibitors (Sigma-Aldrich). After sonication at 4 °C for 20 s, protein concentrations were determined by a bicinchoninic acid (BCA) protein assay kit (Pierce/Thermo Scientific, Pittsburgh, PA, USA). Homogenized protein samples were separated on 4–12% NuPAGE gels (Invitrogen) and transferred to a PVDF membrane. Membranes were incubated with antibodies against the indicated proteins. Immunoreactivity was determined by enhanced chemiluminescence (GE Healthcare Bio-Sciences, Pittsburgh, PA, USA). The images were captured using a bioimaging analyzer (LAS-3000; Fuji, Tokyo, Japan) and analyzed with a Multi-Gauge program (Fuji). Antibodies for western blot analysis were purchased; anti-Aβ antibody (6E10; monoclonal antibody, Signet Laboratories, Dedham, MA, USA), anti-PS antibody, anti-CB antibody, anti-tubulin monoclonal antibody, anti-Drp1 antibody (Santa Cruz Biotechnologies, Santa Cruz, CA, USA), anti-Fis1 antibody, anti-Mfn1 antibody, anti-OPA1 antibody, anti-Bcl-2 antibody, anti-Bax antibody, anti-Bcl-xL antibody, anti-NMDAR1 antibody, anti-NR2A antibody, anti-GluR1 antibody, anti-GluR2 antibody, anti-phospho-ERK antibody, anti-ERK antibody, anti-phospho-CREB Ser133 antibody, anti-CREB Ser133 antibody, anti-synaptophysin antibody and anti-PSD-95 antibody were used for immunoblotting.

CytC activity. Brain tissues were resuspended in hypotonic buffer (10 mM Tris (pH 7.4), 1 mM ethylenediaminetetraacetic acid and 1 mM EGTA) including protease inhibitor cocktail (100 mg/ml phenylmethylsulfonyl fluoride (PMSF), 2 mg/ml leupeptin and 2 mg/ml aprotinin, all from Sigma-Aldrich). After incubation on ice for 30 min, swelled cells were disrupted with 25 strokes of a tight-fitting pestle in a Dounce homogenizer, followed by centrifugation at 500 *g* for 15 min. Supernatants were centrifuged at 17 000 $\times$ *g* for 30 min and upper layers (cytosolic extracts) were isolated. Cytosolic CytC prepared from tissues was subjected to ELISA according to the manufacturer's instruction (Cytochrome c Kit, Invitrogen).

Annexin V FITC staining. Annexin V/PI staining (BD, San Diego, CA, USA) was performed using flow cytometry according to the manufacturer's guidelines. To examine the stage of apoptotic cells, the measurements were carried out. Briefly, subicular cells were trypsinized and collected and stained in solution with annexin V-fluorescein isothiocyanate or PI for 15 min at 25 °C in the dark, and were then washed with ice-cold PBS. Flow cytometry analysis was immediately performed using a FACS Calibur (BD Bioscience, San Jose, CA, USA).

Quantification of immunoreactivity. Four sections (100 μm apart) from Tg and CBKOTg mice were used for this analysis. Immunofluorescence images of the cerebral frontal cortex and hippocampus were taken using a fluorescence microscope (FluoView FV 10i; OLYMPUS). To analyze the amyloid plaque burden, NeuN, and pCREB, the number of immunofluorescence-positive pixels in the subiculum area from the acquired images was analyzed using the Image J processing software (National Institutes of Health, Bethesda, MD, USA).

Statistical analysis. All data are expressed as mean $\pm$ S.E.M. Statistical analysis was performed using GraphPad Prizm4 (San Diego, CA, USA). The data were analyzed by one-way analysis of variance with *post-hoc* test or unpaired *t*-tested regarded as appropriate ($^*P<0.05$ and $^{***}P<0.001$).

Conflict of Interest

The authors declare no conflict of interest.

Acknowledgements. This work was supported by grants from National Research Foundation (2012R1A2A1A01002881, 2013M3C7A1069644), Medical Research Center (2011-0030738), Korean National Institute of Health ROAD R&D Program Project (A092058), for I M-J; and Institute for Basic Science (CA1308), for DH.

1. Nagy Z, Esiri MM, Joachim C, Jobst KA, Morris JH, King EM *et al.* Comparison of pathological diagnostic criteria for Alzheimer disease. *Alzheimer Dis Assoc Disord* 1998; **12**: 182–189.
2. Hardy J, Selkoe DJ. The amyloid hypothesis of Alzheimer's disease: progress and problems on the road to therapeutics. *Science* 2002; **297**: 353–356.
3. Hirai K, Aliev G, Nunomura A, Fujioka H, Russell RL, Atwood CS *et al.* Mitochondrial abnormalities in Alzheimer's disease. *J Neurosci* 2001; **21**: 3017–3023.
4. Palotas A, Kalman J, Palotas M, Juhasz A, Janka Z, Penke B. Fibroblasts and lymphocytes from Alzheimer patients are resistant to beta-amyloid-induced increase in the intracellular calcium concentration. *Prog Neuropsychopharmacol Biol Psychiatry* 2002; **26**: 971–974.
5. Foster TC, Kumar A. Calcium dysregulation in the aging brain. *Neuroscientist* 2002; **8**: 297–301.
6. Heizmann CW, Braun K. Changes in Ca(2+)-binding proteins in human neurodegenerative disorders. *Trends Neurosci* 1992; **15**: 259–264.
7. Baimbridge KG, Celio MR, Rogers JH. Calcium-binding proteins in the nervous system. *Trends Neurosci* 1992; **15**: 303–308.
8. Guo Q, Christakos S, Robinson N, Mattson MP. Calbindin D28k blocks the proapoptotic actions of mutant presenilin 1: reduced oxidative stress and preserved mitochondrial function. *Proc Natl Acad Sci USA* 1998; **95**: 3227–3232.
9. Wernyj RP, Mattson MP, Christakos S. Expression of calbindin-D28k in C6 glial cells stabilizes intracellular calcium levels and protects against apoptosis induced by calcium ionophore and amyloid beta-peptide. *Brain Res Mol Brain Res* 1999; **64**: 69–79.
10. Jung EM, An BS, Choi KC, Jeung EB. Apoptosis- and endoplasmic reticulum stress-related genes were regulated by estrogen and progesterone in the uteri of calbindin-D(9k) and -D(28k) knockout mice. *J Cell Biochem* 2012; **113**: 194–203.
11. Palop JJ, Jones B, Kekonius L, Chin J, Yu GQ, Raber J *et al.* Neuronal depletion of calcium-dependent proteins in the dentate gyrus is tightly linked to Alzheimer's disease-related cognitive deficits. *Proc Natl Acad Sci USA* 2003; **100**: 9572–9577.
12. Airaksinen MS, Eilers J, Garaschuk O, Thoenen H, Konnerth A, Meyer M. Ataxia and altered dendritic calcium signaling in mice carrying a targeted null mutation of the calbindin D28k gene. *Proc Natl Acad Sci USA* 1997; **94**: 1488–1493.
13. Farre-Castany MA, Schwaller B, Gregory P, Barski J, Mariethoz C, Eriksson JL *et al.* Differences in locomotor behavior revealed in mice deficient for the calcium-binding proteins parvalbumin, calbindin D-28k or both. *Behav Brain Res* 2007; **178**: 250–261.
14. Oakley H, Cole SL, Logan S, Maus E, Shao P, Craft J *et al.* Intraneuronal beta-amyloid aggregates, neurodegeneration, and neuron loss in transgenic mice with five familial Alzheimer's disease mutations: potential factors in amyloid plaque formation. *J Neurosci* 2006; **26**: 10129–10140.

15. Iritani S, Niizato K, Emson PC. Relationship of calbindin D28K-immunoreactive cells and neuropathological changes in the hippocampal formation of Alzheimer's disease. *Neuropathology* 2001; **21**: 162–167.
16. Moon M, Hong HS, Nam DW, Baik SH, Song H, Kook SY *et al.* Intracellular amyloid-beta accumulation in calcium-binding protein-deficient neurons leads to amyloid-beta plaque formation in animal model of Alzheimer's disease. *J Alzheimer's Dis* 2012; **29**: 615–628.
17. Janus C, Westaway D. Transgenic mouse models of Alzheimer's disease. *Physiol Behav* 2001; **73**: 873–886.
18. Kobayashi DT, Chen KS. Behavioral phenotypes of amyloid-based genetically modified mouse models of Alzheimer's disease. *Genes Brain Behav* 2005; **4**: 173–196.
19. Sutherland MK, Somerville MJ, Yoong LK, Bergeron C, Haussler MR, McLachlan DR. Reduction of vitamin D hormone receptor mRNA levels in Alzheimer as compared to Huntington hippocampus: correlation with calbindin-28k mRNA levels. *Brain Res Mol Brain Res* 1992; **13**: 239–250.
20. Dowd DR, MacDonald PN, Komm BS, Haussler MR, Miesfeld RL. Stable expression of the calbindin-D28K complementary DNA interferes with the apoptotic pathway in lymphocytes. *Mol Endocrinol* 1992; **6**: 1843–1848.
21. Frank S, Gaume B, Bergmann-Leitner ES, Leitner WW, Robert EG, Catez F *et al.* The role of dynamin-related protein 1, a mediator of mitochondrial fission, in apoptosis. *Dev Cell* 2001; **1**: 515–525.
22. Sultana R, Boyd-Kimball D, Poon HF, Cai J, Pierce WM, Klein JB *et al.* Redox proteomics identification of oxidized proteins in Alzheimer's disease hippocampus and cerebellum: an approach to understand pathological and biochemical alterations in AD. *Neurobiol Aging* 2006; **27**: 1564–1576.
23. Yao J, Irwin RW, Zhao L, Nilsen J, Hamilton RT, Brinton RD. Mitochondrial bioenergetic deficit precedes Alzheimer's pathology in female mouse model of Alzheimer's disease. *Proc Natl Acad Sci USA* 2009; **106**: 14670–14675.
24. Danial NN, Korsmeyer SJ. Cell death: critical control points. *Cell* 2004; **116**: 205–219.
25. Brookes PS, Yoon Y, Robotham JL, Anders MW, Sheu SS. Calcium, ATP, and ROS: a mitochondrial love-hate triangle. *Am J Physiol Cell Physiol* 2004; **287**: C817–C833.
26. Cha MY, Han SH, Son SM, Hong HS, Choi YJ, Byun J *et al.* Mitochondria-specific accumulation of amyloid beta induces mitochondrial dysfunction leading to apoptotic cell death. *PLoS One* 2012; **7**: e34929.
27. Blass JP, Sheu RK, Gibson GE. Inherent abnormalities in energy metabolism in Alzheimer disease. Interaction with cerebrovascular compromise. *Ann N Y Acad Sci* 2000; **903**: 204–221.
28. Calkins MJ, Manczak M, Mao P, Shirendeb U, Reddy PH. Impaired mitochondrial biogenesis, defective axonal transport of mitochondria, abnormal mitochondrial dynamics and synaptic degeneration in a mouse model of Alzheimer's disease. *Hum Mol Genet* 2011; **20**: 4515–4529.
29. Ghosh A, Greenberg ME. Calcium signaling in neurons: molecular mechanisms and cellular consequences. *Science* 1995; **268**: 239–247.
30. Yamin G. NMDA receptor-dependent signaling pathways that underlie amyloid beta-protein disruption of LTP in the hippocampus. *J Neurosci Res* 2009; **87**: 1729–1736.
31. Bliss TV, Collingridge GL. A synaptic model of memory: long-term potentiation in the hippocampus. *Nature* 1993; **361**: 31–39.
32. Molinari S, Battini R, Ferrari S, Pozzi L, Killcross AS, Robbins TW *et al.* Deficits in memory and hippocampal long-term potentiation in mice with reduced calbindin D28K expression. *Proc Natl Acad Sci USA* 1996; **93**: 8028–8033.
33. Adams JP, Sweatt JD. Molecular psychology: roles for the ERK MAP kinase cascade in memory. *Annu Rev Pharmacol Toxicol* 2002; **42**: 135–163.
34. Shaywitz AJ, Greenberg ME. CREB: a stimulus-induced transcription factor activated by a diverse array of extracellular signals. *Annu Rev Biochem* 1999; **68**: 821–861.
35. Pasti L, Carmignoto G, Pozzan T, Battini R, Ferrari S, Lally G *et al.* Cellular calcium handling in brain slices from calbindin D28k-deficient mice. *Neuroreport* 1999; **10**: 2367–2372.
36. Greene JR, Radenahmad N, Wilcock GK, Neal JW, Pearson RC. Accumulation of calbindin in cortical pyramidal cells with ageing; a putative protective mechanism which fails in Alzheimer's disease. *Neuropathol Appl Neurobiol* 2001; **27**: 339–342.
37. Apostolova LG, Dutton RA, Dinov ID, Hayashi KM, Toga AW, Cummings JL *et al.* Conversion of mild cognitive impairment to Alzheimer disease predicted by hippocampal atrophy maps. *Arch Neurol* 2006; **63**: 693–699.
38. Scorrano L, Ashiya M, Buttle K, Weiler S, Oakes SA, Mannella CA *et al.* A distinct pathway remodels mitochondrial cristae and mobilizes cytochrome c during apoptosis. *Dev Cell* 2002; **2**: 55–67.
39. Youle RJ, Karbowski M. Mitochondrial fission in apoptosis. *Nat Rev Mol Cell Biol* 2005; **6**: 657–663.
40. Benard G, Bellance N, James D, Parrone P, Fernandez H, Letellier T *et al.* Mitochondrial bioenergetics and structural network organization. *J Cell Sci* 2007; **120**(Pt 5): 838–848.
41. Costa V, Giacomello M, Hudec R, Lopreiato R, Ermak G, Lim D *et al.* Mitochondrial fission and cristae disruption increase the response of cell models of Huntington's disease to apoptotic stimuli. *EMBO Mol Med* 2010; **2**: 490–503.
42. Nakanishi S. Molecular diversity of glutamate receptors and implications for brain function. *Science* 1992; **258**: 597–603.
43. Fukunaga K, Miyamoto E. Role of MAP kinase in neurons. *Mol Neurobiol* 1998; **16**: 79–95.
44. Bading H, Greenberg ME. Stimulation of protein tyrosine phosphorylation by NMDA receptor activation. *Science* 1991; **253**: 912–914.
45. Li Z, Okamoto K, Hayashi Y, Sheng M. The importance of dendritic mitochondria in the morphogenesis and plasticity of spines and synapses. *Cell* 2004; **119**: 873–887.
46. Barsoum MJ, Yuan H, Gerencser AA, Liot G, Kushnareva Y, Graber S *et al.* Nitric oxide-induced mitochondrial fission is regulated by dynamin-related GTPases in neurons. *EMBO J* 2006; **25**: 3900–3911.
47. Pozueta J, Lefort R, Shelanski ML. Synaptic changes in Alzheimer's disease and its models. *Neuroscience* 2012; **251**: 51–65.
48. Kim JH, Lee JA, Song YM, Park CH, Hwang SJ, Kim YS *et al.* Overexpression of calbindin-D28K in hippocampal progenitor cells increases neuronal differentiation and neurite outgrowth. *FASEB J* 2006; **20**: 109–111.
49. Bellido T, Huening M, Raval-Pandya M, Manolagas SC, Christakos S. Calbindin-D28k is expressed in osteoblastic cells and suppresses their apoptosis by inhibiting caspase-3 activity. *J Biol Chem* 2000; **275**: 26328–26332.
50. D'Amelio M, Cavallucci V, Middei S, Marchetti C, Pacioni S, Ferri A *et al.* Caspase-3 triggers early synaptic dysfunction in a mouse model of Alzheimer's disease. *Nat Neurosci* 2011; **14**: 69–76.
51. Ohno M, Chang L, Tseng W, Oakley H, Citron M, Klein WL *et al.* Temporal memory deficits in Alzheimer's mouse models: rescue by genetic deletion of BACE1. *Eur J Neurosci* 2006; **23**: 251–260.
52. Quackenbush J. Microarray data normalization and transformation. *Nat Genet* 2002; **32**(Suppl): 496–501.
53. Chae S, Ahn BY, Byun K, Cho YM, Yu MH, Lee B *et al.* A systems approach for decoding mitochondrial retrograde signaling pathways. *Sci Signal* 2013; **6**: rs4.
54. Hwang D, Rust AG, Ramsey S, Smith JJ, Leslie DM, Weston AD *et al.* A data integration methodology for systems biology. *Proc Natl Acad Sci USA* 2005; **102**: 17296–17301.
55. Rosenfeld J, Capdevielle J, Guillemot JC, Ferrara P. In-gel digestion of proteins for internal sequence analysis after one- or two-dimensional gel electrophoresis. *Anal Biochem* 1992; **203**: 173–179.
56. Keller A, Nesvizhskii AI, Kolker E, Aebersold R. Empirical statistical model to estimate the accuracy of peptide identifications made by MS/MS and database search. *Anal Chem* 2002; **74**: 5383–5392.
57. Nesvizhskii AI, Keller A, Kolker E, Aebersold R. A statistical model for identifying proteins by tandem mass spectrometry. *Anal Chem* 2003; **75**: 4646–4658.
58. Fu X, Gharib SA, Green PS, Aitken ML, Frazer DA, Park DR *et al.* Spectral index for assessment of differential protein expression in shotgun proteomics. *J Proteome Res* 2008; **7**: 845–854.
59. Ekins S, Nikolsky Y, Bugrim A, Kirillov E, Nikolskaya T. Pathway mapping tools for analysis of high content data. *Methods Mol Biol* 2007; **356**: 319–350.

Supplementary Information accompanies this paper on Cell Death and Differentiation website (http://www.nature.com/cdd)